Semiclassical features in the quantum description of a Dirac particle in a cavity

S. C. Phatak*
Physics Department, Oregon State University, Corvallis, Oregon 97331

Santanu Pal
Variable Energy Cyclotron Centre, 1/AF Bidhannagar, Calcutta 700 064, India

Debabrata Biswas
Theoretical Physics Division, Bhabha Atomic Research Centre, Bombay 400 085, India
(Received 9 May 1994; revised manuscript received 26 September 1994)

The question of classical correspondence in the case of the Dirac equation has not been fully resolved as yet. In this paper, we consider Dirac particles in cavities of various shapes and provide numerical evidence of the influence of periodic orbits in the quantal density of states, $d(E)$. Interestingly, the orbit lengths seem to be the same as in the (scalar) spinless case, though the associated phases in the periodic orbit sum for $d(E)$ are in general different. We also study the spectral fluctuations and find that statistical measures reflect an order-to-chaos transition in the underlying classical dynamics, similar to that seen in the scalar case. We provide a detailed study of the wave functions as well and find, apart from other characteristic features, the existence of scarred states. Typical irregular eigenfunction components, however, exhibit contour splitting and have a Gaussian amplitude distribution.

PACS number(s): 05.45.+b, 03.65.−w

I. INTRODUCTION

The last couple of decades have witnessed a revival of interest in semiclassical methods applied to quantum systems. The importance of such studies stems from the fact that generic classical systems are indeed nonintegrable or irregular, and in such cases direct semiclassical techniques such as the Bohr-Sommerfeld theory or the Einstein-Brillouin-Keller (EBK) quantization schemes [1] do not work. This gap has, however, been bridged to a large extent for spinless particles with the formulation of the periodic orbit theory by Gutzwiller [2] and Balian and Bloch [3]. Thus the density of states can be expressed as a smooth average part superposed with fluctuations that arise as a sum over contributions from all periodic orbits of the underlying classical system. This is true for integrable systems as well [4] though the influence of periodic orbit families differs from that of isolated trajectories. A difficulty in this global scheme, however, lies in its practical implementation since it requires the enumeration of the lengths and stability indices of periodic orbits. Recent studies thus focus on viable quantization methods [5] though the duality in the classical length and quantal energy spectrum is now well established for the spinless case.

Our interest here lies in relativistic quantum systems having spin. In contrast to the nonrelativistic case for scalar particles, where the semiclassical mechanics is now well known, the Dirac Hamiltonian for a relativistic particle does not lend itself directly to a classical description in the correspondence limit, essentially because spin is a quantum variable without a classical analogue. A classical model for electron was first obtained by Barut and Zanghi [6] who accommodated spin by introducing conjugate classical spinor variables in addition to the conjugate variables (x,p) in $3+1$ dimensions. The resulting classical dynamical equations described the motion of an electron in $4+1$ dimensions. The propagator of a Dirac particle was subsequently obtained [7] as a path integral over classical action S in the form $\int e^{iS}$, which is a matrix since it is necessary to specify not only the end points of the path in spatial coordinates, but also the internal spin degrees of freedom. It should then be possible to obtain the density of quantum states in terms of classical actions from the trace of the Fourier transform of the propagator. Alternatively, starting with the full quantum mechanical Dirac propagator for a particle in a two-dimensional billiard, the average part of the spectral density was obtained [8] by evaluating the trace of the infinite-space Green's function in the lowest order. However, it still remains to extend the semiclassical methods to such matrix propagators to obtain the fluctuating part of the spectral density. Do periodic orbits influence the Dirac eigenspectrum and if so how does it differ from the Schrödinger case? Are statistical measures indicative of the underlying classical dynamics? Similar questions can be posed for the wave functions as well. Do generic nodal patterns, contour plots, and amplitude distributions reflect the nature of the classical system and do short periodic orbits leave their imprint or scars in a fashion similar to the spinless nonrelativistic case? Further, the Dirac wave function is a four-component object and its interpretation in terms of classical orbits in the

*Permanent address: Institute of Physics, Sachivalaya Marg, Bhubaneshwar 751 005, India.

correspondence limit is not obvious. A procedure to decouple the Hamiltonian matrix for multicomponent wave functions was formulated by Littlejohn and Flynn [9–11] using Weyl symbol calculus which was recently [12] used to obtain classical equations of motion for Hamiltonians with a spin-orbit interaction. Earlier, vector wave functions were also considered semiclassically by Balian and Bloch [3]. However, the above procedure has not been applied to the Dirac Hamiltonian so far. We would also like to point out that this procedure requiring diagonalization of the Hamiltonian matrix is highly nontrivial. Neither it is possible to ascertain *a priori* whether the diagonalization scheme would apply to the Dirac Hamiltonian at all. On the other hand, analysis of energy level statistics and wave functions is a simpler task enabling us at the same time to explore the classical features of the Dirac Hamiltonian.

In the present paper, we shall concentrate on the applicability of semiclassical methods to the energy spectra of both integrable and nonintegrable Dirac Hamiltonians. Specifically, we shall study the fluctuation measures of the Dirac spectrum, namely, the nearest neighbor spacing distribution and the spectral rigidity, for a relativistic particle in a cavity. We shall also present a detailed study of the wave functions. We shall find that the characteristic features of the fluctuation measures and the wave functions are similar to those obtained earlier for nonrelativistic spinless systems. Since the nature of the fluctuation measures for nonrelativistic systems can be explained [14–17] semiclassically in terms of the dynamics of the analogue classical systems, the above similarity with the relativistic cases would indicate that semiclassical methods can as well be applied to the Dirac Hamiltonian. Though we would not arrive at the explicit form of the classical analogue of the Dirac Hamiltonian for a particle in a cavity from the present studies, the semiclassical features of the Dirac Hamiltonian would confirm the presence of an underlying classical motion. Further, as the fluctuation measures in nonintegrable systems are quite different from those of the integrable ones, it is essential that we study both before we draw any conclusions regarding classical correspondence of the Dirac equation. This is the chief motivation of this work. The issue is important as subatomic physics involves nonclassical degrees of freedom, spin being the most familiar of these. Semiclassical descriptions, which are intuitively appealing, might therefore lead to a better understanding of such systems.

In the following section, we shall briefly sketch the essential steps to calculate the eigenenergies and eigenfunctions of a Dirac particle in a nonspherical cavity. The fluctuation properties of the eigenenergies will be analyzed in Sec. III. In Sec. IV, the characteristic features of the wave functions will be presented. Section V is the concluding one. In what follows, we set $\hbar=c=1$ and energy is expressed in units of fm^{-1}.

II. DIRAC PARTICLE IN A DEFORMED CAVITY

The system we consider here is a relativistic spin-$\frac{1}{2}$ particle constrained to move in a cavity having quadrupole deformation. Thus it is a three-dimensional billiard having spin. In principle, the calculation can be done for a cavity having arbitrary shape. But the calculations for a quadrupole deformation are somewhat simpler and the essential features of the order-to-chaos transition can be demonstrated by varying the deformation parameter.

A Dirac Hamiltonian in two dimensions ("neutrino billiards") was considered earlier [8] as an example of a time-reversal symmetry breaking system and the energy spectrum was found to be consistent with the statistics of a Gaussian unitary ensemble (GUE). It should be pointed out, however, that the present Hamiltonian in three dimensions is time-reversal symmetric. Moreover, we shall pay particular attention to the role of the periodic orbits to emphasize the semiclassical nature of the spectrum. It may further be clarified at this point that in what follows we shall refer to the classical periodic orbits of the Dirac Hamiltonian in the context of their effect as revealed from the quantum spectrum, and they are not obtained explicitly here from any classical dynamical calculation.

Consider a relativistic spin-$\frac{1}{2}$ particle constrained to move in a cavity represented by a scalar four-potential $V(\vec{r})$. To obtain the eigenenergies and the eigenfunctions we have to solve the Dirac equation:

$$[\vec{\alpha}\cdot\vec{p}+\beta\{m+V(\vec{r})\}]\psi_\varepsilon(\vec{r})=\varepsilon\psi_\varepsilon(\vec{r}) \tag{1}$$

with

$$V(\vec{r})=\begin{cases}0 & \text{for } r\le R(\theta,\phi)\\ \infty & \text{for } r>R(\theta,\phi)\end{cases},$$

where $R(\theta,\phi)$ defines the cavity surface in spherical polar coordinates. The energy eigenvalues will be determined from the linear boundary condition

$$-i\vec{\gamma}\cdot\hat{\vec{n}}\psi_\varepsilon(\vec{r})=\psi_\varepsilon(\vec{r}) \tag{2}$$

at the boundary of the cavity. Here $\hat{\vec{n}}$ is the outward unit normal to the boundary, $\vec{\alpha}$ and β are the Dirac matrices

$$\vec{\alpha}=\begin{bmatrix}0 & \vec{\sigma}\\ \vec{\sigma} & 0\end{bmatrix},\quad \beta=\begin{bmatrix}1 & 0\\ 0 & -1\end{bmatrix}, \tag{3}$$

$\gamma_0=\beta$, and $\vec{\gamma}=\beta\vec{\alpha}$. This boundary condition corresponds to a normal flow of zero current through the cavity surface [13]. It also satisfies the Hermiticity requirement of the Dirac Hamiltonian within the cavity and does not give rise to antiparticles in the classically forbidden region [8]. Further, Eq. (2) corresponds to a specular reflection of the spatial part of an incident Dirac spinor on a flat boundary without flipping the spin [8]. The above boundary condition gives a transcendental equation for the eigenenergy ε. For a spherical cavity of radius R, the conserved quantities are the energy ε, the total spin j, the projection of the spin along the z axis, m_j, and k, which is the eigenvalue of the operator $K=\beta(\vec{\sigma}\cdot\vec{L}+1)$. One can show that $k=\pm(j+\frac{1}{2})$. Thus the eigenstates can be labelled by ε, k, and m_j. The solutions are

$$\psi^k_{\varepsilon,m_j}(\vec{r})=N\begin{bmatrix} j_l(pr) \\ -i\vec{\sigma}\cdot\hat{\vec{r}}Cj_{l'}(pr)\end{bmatrix}\chi^{m_j}_k(\hat{\vec{r}})=N\begin{bmatrix} j_l(pr)\chi^{m_j}_k(\hat{\vec{r}}) \\ -i\vec{\sigma}\cdot\hat{\vec{r}}Cj_{l'}(pr)\chi^{m_j}_k(\hat{\vec{r}})\end{bmatrix}$$
$$=N\begin{bmatrix} j_l(pr) \\ -i\vec{\sigma}\cdot\hat{\vec{r}}Cj_{l'}(pr)\end{bmatrix}\begin{bmatrix} l & \frac{1}{2} & j \\ m_l & m_\sigma & m_j\end{bmatrix}Y_{l,m_l}(\hat{\vec{r}})\chi_{1/2,m_\sigma}\ , \tag{4}$$

where N is the normalization constant, $p=(\varepsilon^2-m^2)^{1/2}$, $k'=-k$, $j_l(pr)$ is the spherical Bessel function, [ ] is the Clebsch-Gordan coefficient for coupling of two angular momenta, Y_{l,m_l} are the spherical harmonics, and $\chi_{1/2,m_\sigma}$ is the two-component Pauli spinor. The constant C in the lower component is $\pm p/(p+m)$ with + (−) sign for k positive (negative). In terms of k, j, l, and l' are given by $j=k-\frac{1}{2}$ $(-k-\frac{1}{2})$, $l=k$ $(-k-1)$, and $l'=k-1$ $(-k)$ for k positive (negative). The energy eigenvalues ε are obtained by solving Eq. (2) above. For a spherical cavity, this implies $j_l(pr)=-Cj_{l'}(pr)$ and eigenvalues of p are obtained by numerically solving this equation. For an arbitrarily shaped cavity, we do not have analytic solutions. We can, however, expand the eigenfunctions in a spherical basis and impose the boundary condition [Eq. (2)] numerically. For an axially symmetric cavity, m_j is still a good quantum number and the eigenfunctions can be written as

$$\psi_{\varepsilon,m_j}(\vec{r})=\sum_k A_k\psi^k_{\varepsilon,m_j}(\vec{r})\ . \tag{5}$$

Choosing the z axis along the axis of symmetry, the boundary condition [Eq. (2)] becomes

$$-i[\vec{\gamma}\cdot\hat{\vec{n}}(\theta)\psi_{\varepsilon,m_j}(\vec{r})]_{r=R(\theta)}=[\psi_{\varepsilon,m_j}(\vec{r})]_{r=R(\theta)}\ . \tag{6}$$

Here, θ is the angle from the symmetry axis. For an arbitrary axially symmetric deformation, the boundary $R(\theta)$ can be expressed in the form

$$R(\theta)=R_0\left[1+\sum_l \alpha_l P_l(\cos\theta)\right] \tag{7}$$

with P_l being the Legendre polynomial. In terms of $R(\theta)$ defined above, $\hat{\vec{n}}$ is

$$\hat{\vec{n}}(\theta)=\frac{\left[\left[1+\sum_l \alpha_l P_l(\cos\theta)\right]\hat{\vec{r}}+\sum_l \alpha_l P_l'(\cos\theta)\sin\theta\,\hat{\theta}\right]}{\left[\left[1+\sum_l \alpha_l P_l(\cos\theta)\right]^2+\left[\sum_l \alpha_l P_l'(\cos\theta)\sin\theta\right]^2\right]^{1/2}}\ . \tag{8}$$

Using Eqs. (4)–(6), the upper component gives

$$\sum_k[\vec{\sigma}\cdot\hat{\vec{n}}(\theta)\vec{\sigma}\cdot\hat{\vec{r}}C_k j_{l'}(pr)\chi^{m_j}_k(\hat{\vec{r}})+\sum_k j_l(pr)\chi^{m_j}_k(\hat{\vec{r}})]_{r=R(\theta)}A_k=0\ . \tag{9}$$

The equation for the lower component is identical. This equation can be converted into a matrix equation by multiplying by $(\chi^{m_j}_{k'})^\dagger$ and integrating over angles. Notice that r in the Bessel functions depend on θ and therefore the integration has to be done numerically. With this, the boundary condition reduces to

$$\sum_k M^{m_j}_{k,k'}(\varepsilon)A_k=0\ . \tag{10}$$

The energy eigenvalue are determined by demanding that the determinant of $M^{m_j}_{k,k'}(\varepsilon)$ vanish and the coefficients A_k are determined by solving Eq. (10) above. The matrix M above is infinite dimensional. In a numerical calculation, M is truncated while ensuring that the energy eigenvalues are stable. For a given range of ε, the eigenvalues (zeros of the determinant) are first located with an absolute accuracy of 10^{-7} using a trial size of M. Subsequently, the dimension of M is increased (typically by adding two more rows and columns) and the eigenvalues are again obtained. If each of the eigenvalues of the new set differs by more than 10^{-5} from the corresponding ones of the earlier set, the dimension of the matrix is increased further till the above criterion is met. Further, we set the mass $m=0$, in order to make the calculation fully relativistic. This is evidently an idealization which is reached in an energy domain where the rest mass of a particle is extremely small compared to the energy values. We also choose the value of R_0 in Eq. (7) to be 1 fm.

III. SPECTRAL FLUCTUATIONS OF THE DIRAC HAMILTONIAN

We shall focus on two aspects of the Dirac eigenspectrum in this section. As for the Schrödinger spectrum, the density of eigenenergies, $d(E)$, for the Dirac spectrum can be expressed as a sum of a smooth average part, $d_{\rm av}(E)$, superposed with fluctuations, $d_{\rm fl}(E)$. Our interest here lies in the nature of the fluctuations. To this end, we shall first carry out a detailed analysis of their statistical properties using commonly used measures such as the nearest neighbor spacing distributions $P(s)$ and the spectral rigidity $\Delta_3(L)$. The motivation here is directly relat-

ed to the known results for the Schrödinger spectrum, where $P(s)$ and $\Delta_3(L)$ belong to universality classes which depend on the nature of the underlying classical dynamics. An obvious question therefore concerns the behavior of fluctuation measures with variation of a parameter which takes the classical dynamics away from integrability.

At a deeper level, the universalities in the Schrödinger spectrum are due to the collective properties of periodic orbits which constitute $d_{\rm fl}(E)$. An unmistakable signature of the semiclassical nature of the spectrum is also the saturation of the spectral rigidity, a phenomenon that does not emerge from random matrix models [14]. We shall therefore look at this aspect as well while studying the statistical properties. Finally, we shall analyze the Fourier transform of the Dirac spectrum in order to obtain a direct proof of the validity of periodic orbit theory for relativistic systems with spin.

The energy spectra E_i for quadrupole deformations [$\alpha_l=0$ for all l except $l=2$; see Eq. (7)] of the cavity were calculated using the method described in the section above. These were subsequently "unfolded" to obtain the sequence ε_n for further analyses. Apart from the spherical cavity, other shapes considered correspond to cavities with $\alpha_2=0.1$ and 0.4.

Using the unfolded spectra, we first present the nearest neighbor level spacing distribution $P(s)$, defined such that $P(s)ds$ is the probability of finding successive levels with spacing between s and $s+ds$. The distribution is shown in Fig. 1 for sequences of given parities and z component of total angular momentum. Now it is already known [15] that for systems with classical integrable motion the levels tend to cluster in the quantum energy spectrum and for generic regular systems the spacing distribution is given as $P(s)=\exp(-s)$, a Poisson distribution. On the other hand, levels tend to repel each other for systems whose classical dynamics is chaotic and it was shown [16] heuristically that the spacing distribution follows the Wigner surmise, $P(s)=(\pi s/2)\exp(-\pi s^2/4)$. Both of these ideal extremes are also shown in this figure. The calculated distributions change from Poisson to Wigner as the deformation increases from $\alpha_2=0.0$ to 0.4 through 0.1, typical of an order-to-chaos transition. The spacing distribution therefore reflects the transition in the classical dynamics and the two extremes ($\alpha_2=0$ and 0.4) belong to the respective universality classes (Poisson and Wigner distributions, respectively) corresponding to regular and chaotic motion.

We next consider the spectral rigidity $\Delta_3(L)$, defined as the average mean square deviation of the spectral staircase $N(E)$ from the best fitting straight line in an interval of L mean level spacings:

$$\Delta_3(L)=\left\langle \min_{a,b} \frac{1}{L}\int_{\varepsilon_0-L/2}^{\varepsilon_0+L/2} d\varepsilon[N(\varepsilon)-a-b\varepsilon]^2 \right\rangle . \tag{11}$$

In the above equation, $N(\varepsilon)$ is the spectral staircase of the unfolded spectrum (mean spacing unity) and $\langle\ \rangle$ denotes local averaging around ε_0. In the Schrödinger case, the expression for the semiclassical density of states in terms of periodic orbits,

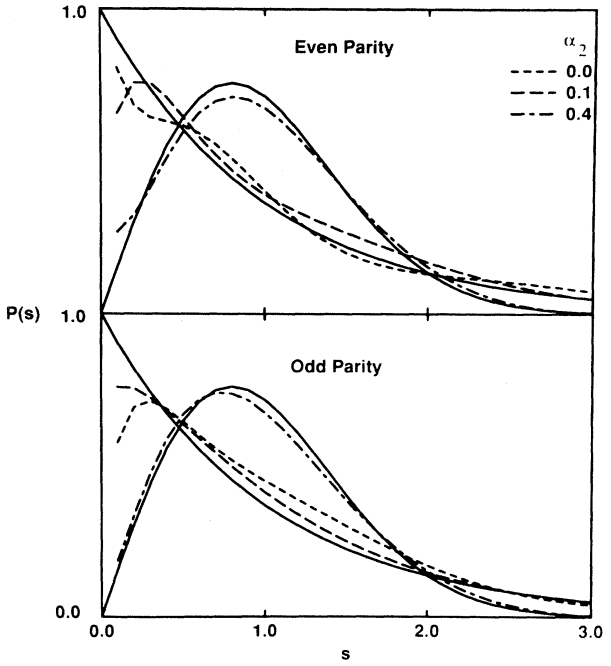

FIG. 1. The nearest neighbor spacing distribution for $\alpha_2=0$, 0.1, and 0.4. The solid lines correspond to the Poisson and Wigner distributions. The upper one is for even parity states while the lower one is for odd parity states.

$$d(E)=d_{\rm av}(E)+\sum_p\sum_r D_{p,r}\cos\{r(S_p-\mu_p)\} , \tag{12}$$

can be used to express the spectral rigidity as [17]

$$\Delta_3(L)=\frac{2}{\hbar^{2\nu}}\int_0^\infty \frac{dT}{T^2}\phi(T)G(LT/2\hbar) , \tag{13}$$

where $G(y)=1-F^2(y)-3[F'(y)]^2$, $F(y)=(\sin y)/y$, and ν takes values 0 or $(N-1)/2$ depending on whether the periodic orbits are isolated or occur in $(N-1)$ parameter families, N being the degrees of freedom. In Eq. (12) above, r is the repetition number of a primitive orbit p whose action and Maslov index are denoted by S_p and μ_p, respectively, while $D_{p,r}$ is the corresponding amplitude. The form factor

$$\phi(T)=\left\langle \sum\sum A_i A_j\cos[(S_i-S_j)/\hbar]\delta\left[T-\frac{T_i+T_j}{2}\right]\right\rangle$$

is crucial in the analysis and embodies the collective properties of periodic orbits. Here S_i and T_i refer to the reduced action and time period of the orbit, A_i is half the amplitude that occurs in Eq. (12), and the subscripts i and j refer to any periodic orbit, primitive or otherwise. For the integrable and chaotic cases, $\phi(T)$ has distinct universality classes [17,18] which manifest directly in $\Delta_3(L)$ for values of $L \ll L_{\rm max}=hd_{\rm av}(E)/T_{\rm min}$. Thus

$$\Delta_3(L)=\begin{cases} L/15\ , & \text{integrable motion} \\ \ln(L)/\pi^2-0.007\ , & \text{chaotic motion with time-reversal symmetry}\ . \end{cases} \tag{14}$$

For large L, the behavior of $\Delta_3(L)$ depends crucially on the orbit selection function $G(y)$ (for a plot, see [17]) which saturates for $y>\pi$. Thus for $L \gg L_{\max}$ the contribution of even the shortest orbit ceases to vary as a function of L and this leads to a saturation in the spectral rigidity. Clearly, this is a direct consequence of the existence of periodic orbits and hence an underlying classical dynamics in the system.

The rigidity obtained from the spectrum of a Dirac particle for all three cases of α_2 is shown in Fig. 2. The regular and fully chaotic limits are also shown. For a spherical cavity, the curve closely follows the $L/15$ line for small L. This is true for a small deformation ($\alpha_2=0.1$) as well for both the even and odd parities, while for $\alpha_2=0.4$ the curve for small L is close to the chaotic limit. These observations are consistent with the results for the nearest neighbor spacing distribution. For larger values of L, the rigidity tends to saturate in all cases. It therefore seems quite likely that the density of states for the Dirac spectrum has fluctuations similar to those in Eq. (12) for the Schrödinger spectrum.

This point can indeed be strengthened by evaluating $L_{\max}$. The frequency of the slowest oscillation in $d_{\rm fl}(E)$, which corresponds to $T_{\min}$, can be determined from a Fourier transform of the spectrum for $m_j=\frac{1}{2}$ and positive and negative parity states considered separately. In Fig. 3, we show plots of the function

$$g(x)=\sum_n \cos(E_n x)\exp(-\eta E_n^2) \tag{15}$$

for $\alpha_2=0$, 0.1, and 0.4. In writing the above form, we have used the fact that $S_p=\int p\,dq=\varepsilon X$ for a mass zero particle of energy ε and an orbit of length X. The damping factor η is introduced keeping in mind the finite stretch of the spectrum available in practice and this leads to a broadening of the peaks. Clearly, there are several peaks indicating the validity of Eq. (12) in the Dirac case. The position of the first peak can thus be used to calculate the value of $L_{\max}$. These are marked in Fig. 2. The values are seen to be consistent with the theoretical predictions for Δ_3 using Eq. (12).

The physical interpretation of the lengths at which peaks occur is thus a question that follows naturally. We thus evaluate $g(x)$ in Eq. (15) using both parities (the effect of parity selection [19] is obvious in Fig. 3) and all allowed projections of the total angular momentum. Our results are displayed in Figs. 4 and 5 for $\alpha_2=0$ and 0.4, respectively. The lengths of periodic orbits for a spinless nonrelativistic particle are also marked for values of

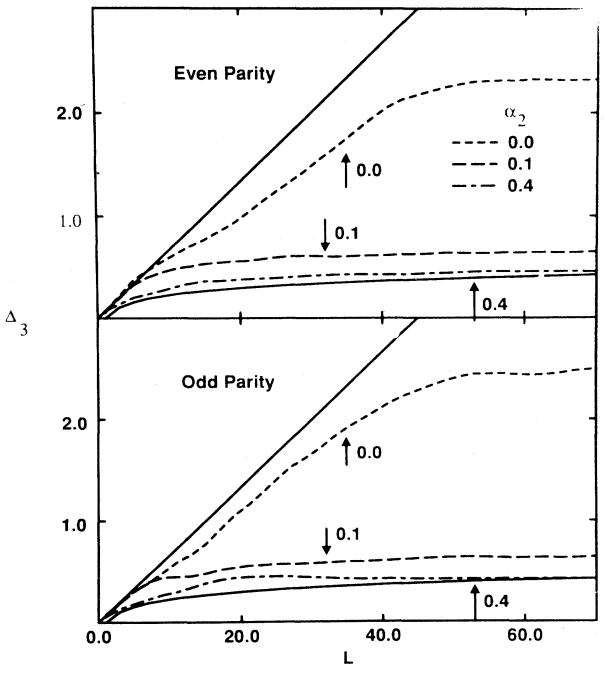

FIG. 2. The spectral rigidity $\Delta_3(L)$ for the three shapes as in Fig. 1. The solid lines correspond to the integrable (straight line) and chaotic limits. The arrows indicate the values of $L_{\max}$. The upper one is for even parity states while the lower one is for odd parity states.

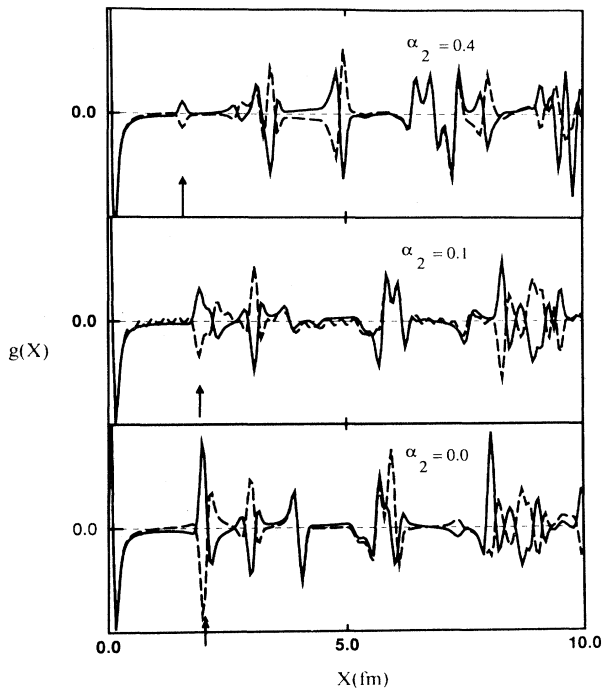

FIG. 3. The Fourier transform of the $m_j=\frac{1}{2}$ even (dashed) and odd (solid line) states for $\alpha_2=0$ (bottom), 0.1 (middle), and 0.4 (top). The position of the first peak is marked.

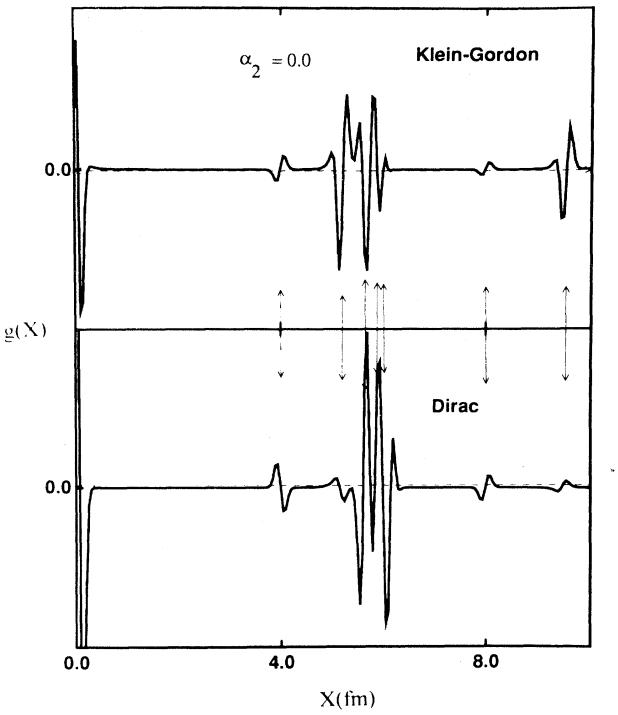

FIG. 4. The Fourier transform of the combined spectra for the spherical cavity. Both the Dirac and Klein-Gordon (KG) cases are shown.

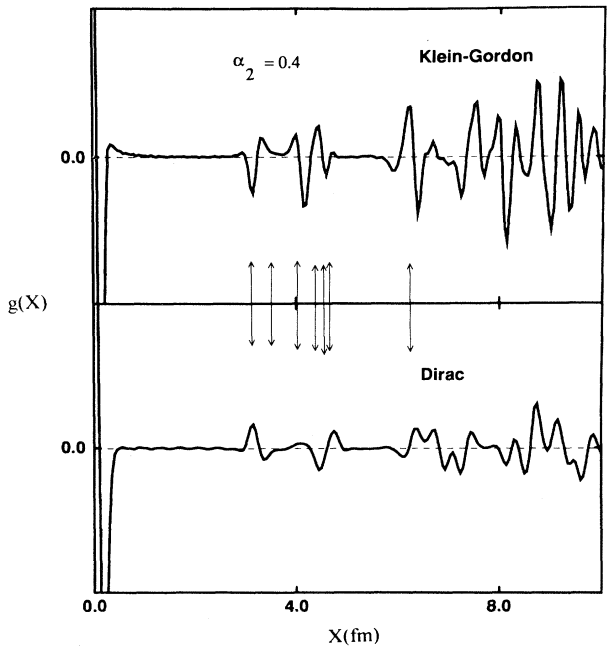

FIG. 5. As in Fig. 4, for $\alpha_2=0.4$.

$x<10$. For $\alpha_2=0$, the periodic orbits in the equatorial plane are of shapes such as equilateral triangle, square, pentagon, hexagon, and so on, corresponding to respective path lengths such as 5.196, 5.657, 5.878, and 6, and so on, in addition to the shortest path of length 4 along the diameters. The function $g(x)$ has a distinct behavior at these positions (for a discussion of shapes, see Ref. [20]) though the width associated with η makes it difficult to separate the last two. Distinct peaks can also be seen at $x=8$ and around 9.5, corresponding to a repetition of the orbit of length 4 and a pentagram orbit of length 9.51.

Thus the peak positions physically correspond to the length of classical periodic orbits in the cavity. Notice also the distinct shapes for the shortest orbit ($x=4$) and its repetition at $x=8$. In the first case, there is an initial positive peak and then a sharp drop resulting in a negative peak which decays to zero. The behavior is reversed at $x=8$ indicating that phases in $d_{\mathrm{fl}}(E)$ occur as in Eq. (12) (i.e., in multiples of the repetition number) and are not equal to 2π. This is in contrast to the expression for the semiclassical density of states for the Schrödinger equation of a two-dimensional billiard, where all phases are equal to $\pi/4$ [2]. In the present case (massless particle), however, we compare the behavior with the Klein-Gordon (KG) spectrum whose Fourier transform is also shown in Fig. 4. Clearly, at the periodic orbit lengths, the curve for $g(x)$ has a distinct behavior. Moreover, the shapes at all lengths appear to be the same, indicating that the phases are homogeneous.

Another aspect worth noting is the decrease in height of the peak with repetition number. Compare for example, the height of the negative peak at $x=4$ and positive peak at $x=8$. Clearly, the former is $\sqrt{2}$ times the latter ($r=2$, where r is the repetition number) indicating that the amplitude decreases with repetition number as in the nonrelativistic spinless case for orbits occurring in families.

Thus there is enough evidence that the periodic orbit sum for the Dirac density of states is similar to the spinless case and the difference essentially arises in the actions S due to the additional contributions from the dynamics of the spin variables, which give rise to entirely distinct spectra.

As for the spherical case, the spectra of deformed cavities are also influenced by periodic orbits. For $\alpha_2=0.4$, they appear at $x=3.1$, 4.026, 4.384, 4.55, 4.65, 6.25, and so on. All except the last one are orbits occurring in one-parameter families in the XY plane at $Z=0$. The path of length 6.25 is for a parallelogram connecting the four tips of the major and minor axes. The presence of these orbits in $d_{\mathrm{fl}}(E)$ can be seen in Fig. 5. The path of length 5.42 along the symmetry (Z) axis is, however, not as distinct since it is isolated and unstable and hence seems to have a smaller weight compared to others, as in the Schrödinger case. There is also an orbit of length 3.52 which is in the XY plane and oscillates between opposite points at a nonzero Z value where the curvature is zero. The plot of $g(x)$ using the KG spectrum is also shown in Fig. 5 for $\alpha_2=0.4$. Clearly the same orbits influence the Dirac and KG spectra though the corresponding phases μ_p are distinct for the two.

IV. WAVE FUNCTIONS

Having established the influence of classical dynamics in the eigenenergy spectrum of a Dirac particle in both the spherical and nonspherical cavities, it is natural to enquire about the nature of the wave functions in such cases. As in the case of fluctuation measures, we shall confine ourselves to those properties which are known to reflect the nature of the underlying classical dynamics. Of these, nodal and contour plots offer considerable insight and we shall use these extensively in our investigation of "scarred" states. The amplitude distribution and the phenomenon of "contour splitting" are two other characteristics that are known to have a direct relationship with the underlying classical dynamics and we shall present our results on these for both the spherical and deformed cavities.

The eigenfunctions for quadrupole deformations of the cavity are calculated by using the method described in Sec. II above. The eigenfunctions consist of four components. We shall call these ψ_i with i running from 1 to 4. The first two are given by the upper component of the Dirac eigenfunction with m_σ equal to $+\frac{1}{2}$ and $-\frac{1}{2}$, respectively, and the last two are given by the lower component, also with m_σ values of $+\frac{1}{2}$ and $-\frac{1}{2}$. The lower two components are essentially obtained by operating $\vec{\sigma}\cdot\vec{\nabla}$ on the upper components. We shall therefore consider the first two components only for the discussion.

A. Nodal patterns

Nodal patterns, along with the amplitude distribution and spatial correlation function, were the first characteristics that were studied in detail [21]. An important, though not unmistakable, signature of classical nonintegrability in a nodal pattern is the presence of avoided crossings. It is also known that such a phenomenon can occur in integrable systems with degeneracies [22]. However, the presence of nonintegrability does make the pattern "irregular" in sharp contrast to the integrable case.

For the spherical cavity, ψ_1 and ψ_2 are proportional to $j_l(pr)Y_{l,\mu-1/2}(\theta)$ and $j_l(pr)Y_{l,\mu+1/2}(\theta)$, respectively. Thus the nodal lines (the lines along which the wave function vanishes) are given by $j_l(pr)=0$ and $Y_{l,m_l}=0$. These correspond to lines of constant r and constant θ in the polar coordinate system. Furthermore, there is a correlation between the two components; namely, the constant r nodal lines are the same for the two components and there is one less (more) constant θ nodal line for ψ_2 if m_j is positive (negative). The nodal curves for the first component of the negative parity, $m_j=\frac{1}{2}$ state at $\varepsilon=21.2458$ are plotted in Fig. 6. There are no avoided crossings and contour splittings. The corresponding perspective plot of the wave function is shown in Fig. 7. This is clearly the "whispering gallery" mode that is known to exist in the Schrödinger wave functions of the circle billiard. Generally, this mode becomes prominent as $|k|$ becomes large.

As an illustrative example of 0.4 deformation, we present in Figs. 8 and 9 the nodal curves for ψ_1 and ψ_2 of the positive parity, $m_j=\frac{1}{2}$ state at $\varepsilon=36.7397$. These

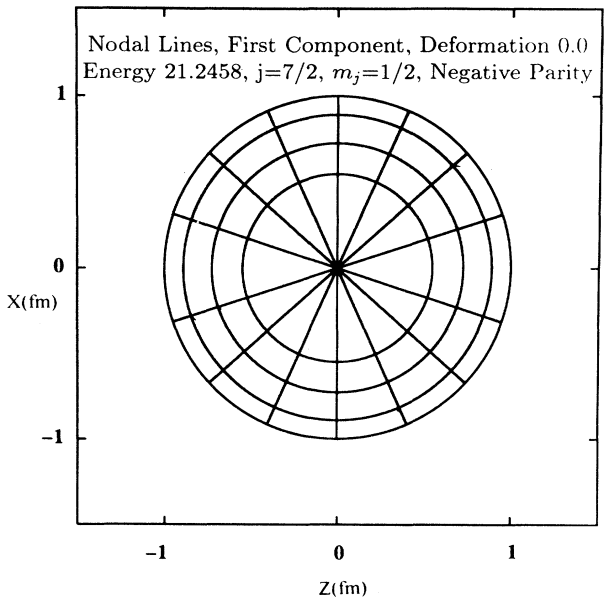

FIG. 6. Nodal curves of ψ_1 in a spherical cavity.

curves are distinct from the zero deformation case and display avoided crossings and are also irregular. The lack of correlation between the two components is also evident here. The corresponding spectral statistics for this system is close to that of chaotic systems. Clearly, then, nodal patterns reflect the underlying irregularity of the classical dynamics.

B. Contour plots and scarred wave functions

We now turn our attention to the phenomenon of scarring. Scarred states are a class of states localized on short unstable periodic orbits that were first seen in the stadium billiard and studied extensively by Heller [23]. The discovery has indeed led to a host of theoretical work of which that by Bogomolny [24], Berry [25], and Eckhardt, Hose, and Pollak [26] has attracted considerable attention. In the first two [24,25], the (energy) averaged intensity is expressed as a sum of contributions from periodic orbits. The mechanism, however, is clearly collective and hence not evident from these studies. Eckhardt, Hose, and Pollak [26] introduced the concept of adiabatic stability of (Lyapunov) unstable periodic orbits and showed that short orbits possessing this quality generate a dynamic confining potential similar to those constructed for the bouncing ball family of periodic orbits in the stadium [27] and $\pi/3$ rhombus billiard [28]. Scarred states can thus be predicted to an extent using such analysis for the quartic oscillator. However, the theory has not been tested on other systems, and, in general, the scarring mechanism is still poorly understood.

Our primary interest here is to numerically establish the existence of scarred eigenfunctions for the Dirac equation. For the spherical cavity, the "whispering gallery" mode shown earlier is clearly an example of localization. However, in this case the orbits do not occur in

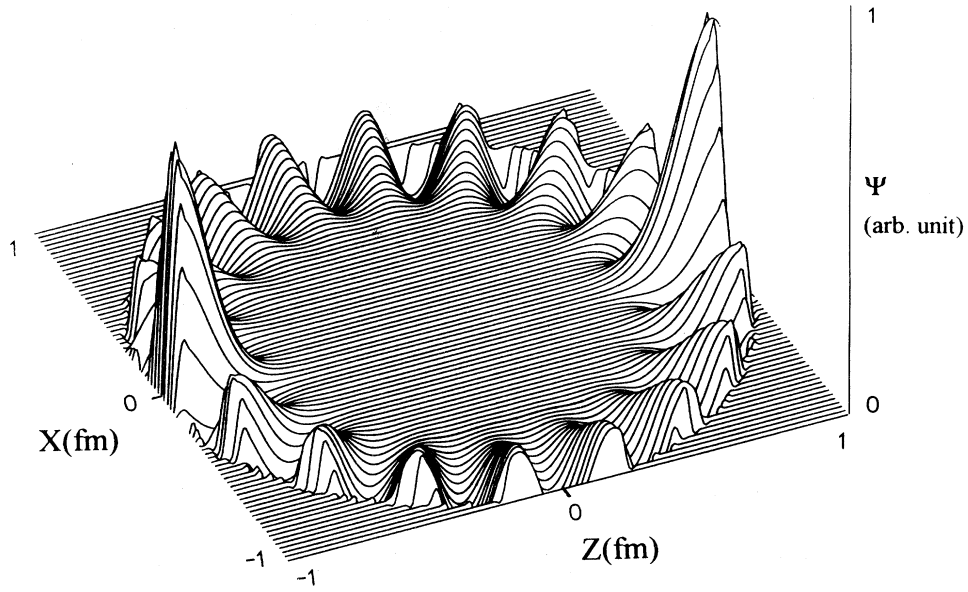

FIG. 7. Perspective plot of ψ_1 used in Fig. 6.

two-parameter families. With the introduction of a slight deformation, however, the structure of orbits changes, and a wider class of localized states can be observed.

Figure 10 shows an example of scarring on an isolated orbit for the 0.1 deformation cavity. Two conjugate (focal) points can also be observed and the behavior is similar to that of some of the eigenfunctions in the stadium billiard. Note also that the oscillation around the orbit is identical to the schematic plot of Bogomolny (see [24]). Another example of scarring on the same orbit can be seen in Fig. 11 though having a visibly different structure.

The effect becomes even more dramatic and pronounced for a larger deformation ($\alpha_2=0.4$). The whispering gallery modes are visible again as can be seen in Fig. 12 for a high m_j state. For the orbit along the z axis, also, we have observed a number of scarred states with a variety of structures. However, there are other states where localization is very strong, though not pronounced on any particular orbit. One such example can be seen in Fig. 13. Finally we have in Fig. 14 the contour

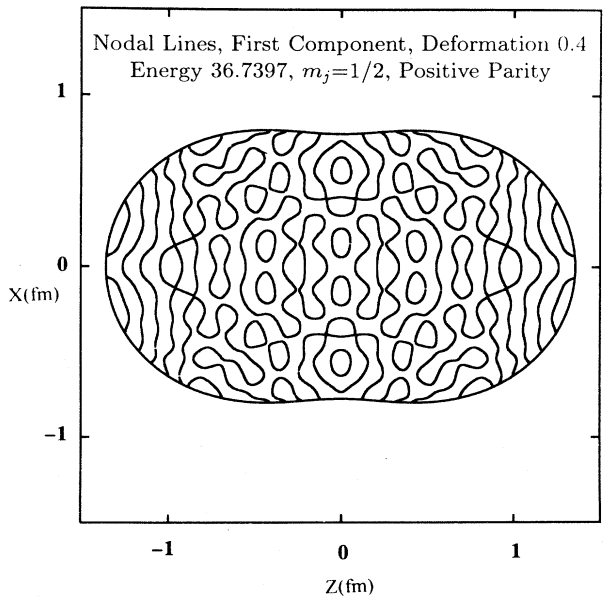

FIG. 8. Typical nodal curves of ψ_1 for $\alpha_2=0.4$.

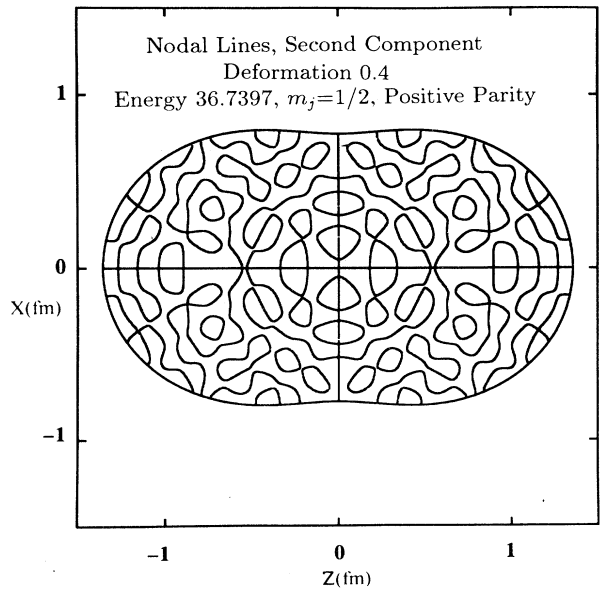

FIG. 9. As in Fig. 8 for the second component.

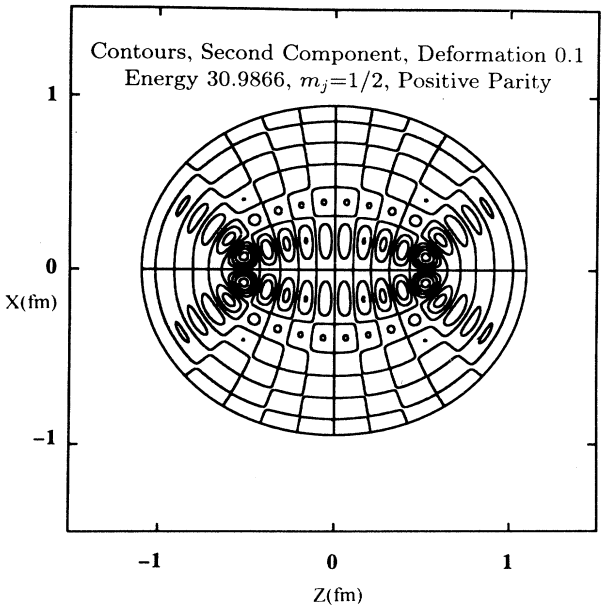

FIG. 10. Scarring on an isolated orbit in the $\alpha_2=0.1$ cavity.

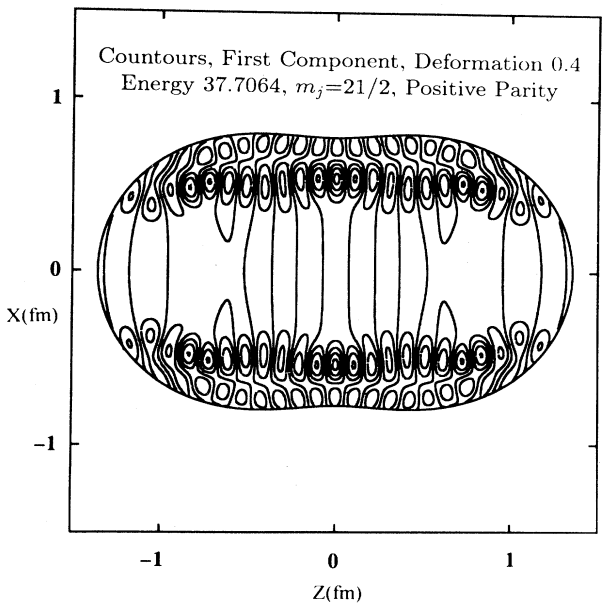

FIG. 12. A whispering gallery mode in the $\alpha_2=0.4$ cavity. The first component is shown here.

plots of a state at $\varepsilon=37.9907$ with scarring on the diamond shaped orbit connecting the tips of the major and minor axes.

We have thus demonstrated the existence of scarred eigenfunctions for a Dirac particle in a nonspherical cavity. The kinds of structures seen are reminiscent of the wave functions of the Schrödinger equation, an observation consistent with the earlier section on spectral statistics.

C. Amplitude distribution $P(\psi)$ and contour splitting

The amplitude distribution [29] has been used in several studies to judge the degree of irregularity in the Schrödinger eigenfunctions of nonintegrable systems. The initial motivation came from an extension of the finite superposition of plane waves applicable to integrable systems. For chaotic systems, keeping in mind the

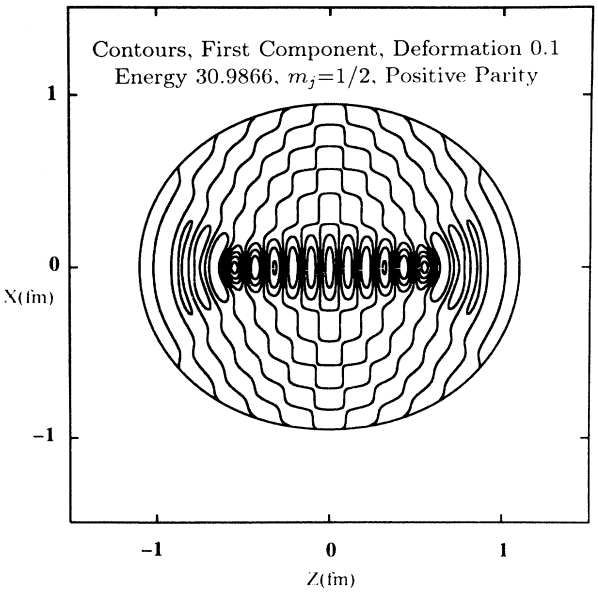

FIG. 11. Another example of scarring on the same orbit as in Fig. 10. Note the visibility different structure.

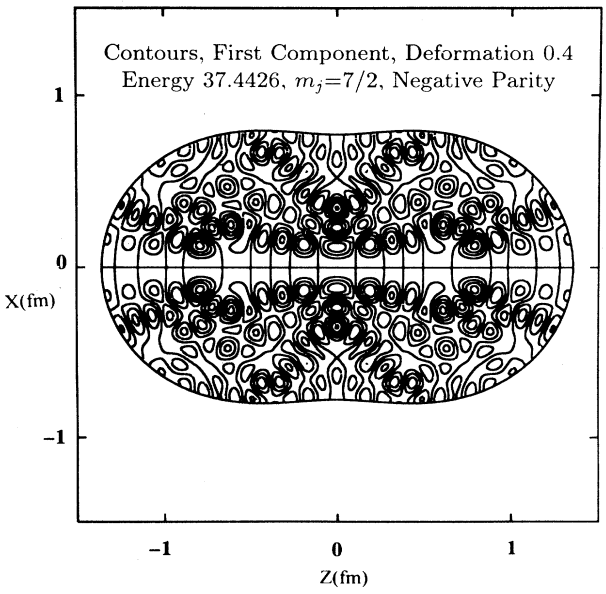

FIG. 13. An example of scarring by more than one orbit.

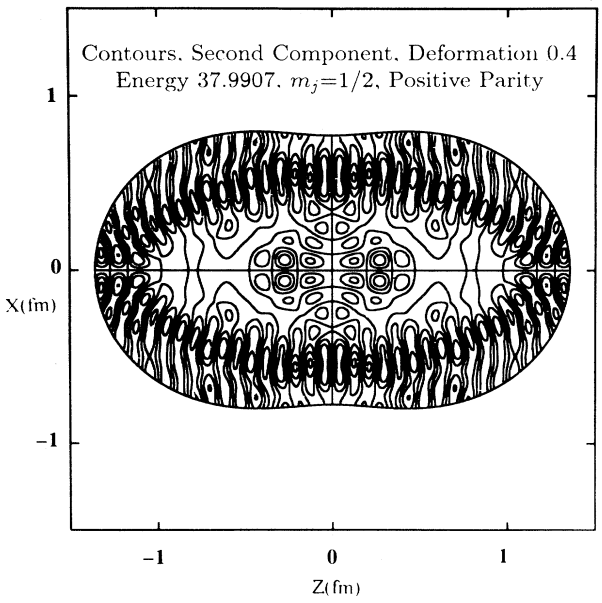

FIG. 14. Scarring along a diamond shaped orbit.

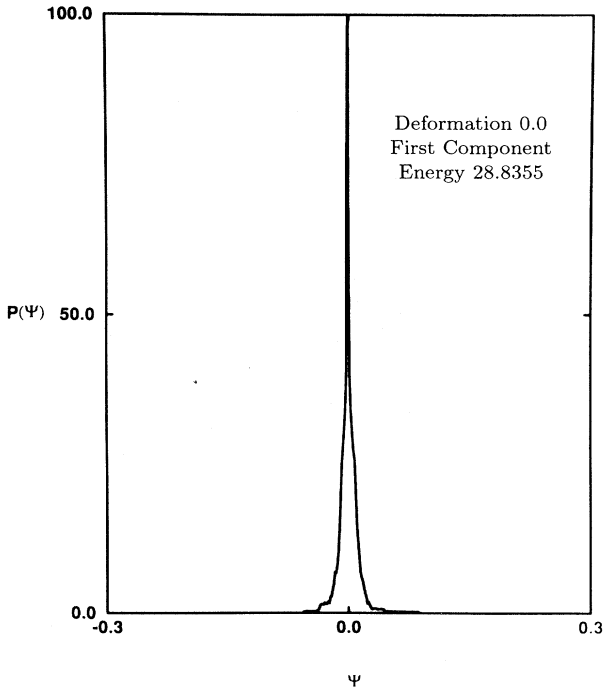

FIG. 15. The amplitude distribution $P(\psi)$ for a typical state in the spherical cavity.

isotropy of momentum directions swept by a typical orbit, Berry [29] proposed an ansatz using an infinite superposition of waves with the same wave vector magnitude but random phases and directions. Each of the components can then be treated as a random variable with identical distribution which then leads to a Gaussian distribution for the amplitude ψ, using the central limit theorem. Though lacking a firm theoretical basis, the conclusions have indeed been verified, in particular for the stadium billiard [21]. Biswas, Azam, and Lawande [30] have subsequently used the periodic orbit approach along with a couple of limiting theorems on nonidentical distributions (each orbit has indeed a distinct and different contribution as the works of Bogomolny [24] and Berry [25] reveal) to show that for a typical unscarred state, where a large number of periodic orbits contribute, the amplitude distribution is close to a Gaussian. A scarred state, on the other hand, would have a very sharp peak near $\psi=0$, indicating that the wave function is localized in a small region of the classically allowed configuration space. A typical regular (though nonlocalized as in the rectangular billiard) state, on the other hand, would have smooth but non-Gaussian distribution except for a spike at $\psi=0.0$. The behavior near zero in this case is due to the fact that the number of such points is twice that of a small positive or negative value of ψ.

The above description immediately suggests another measure of irregularity. Irregular wave functions with a Gaussian amplitude distribution should also possess "surface roughness" and show up in the splitting of contours. This concept was introduced recently by Biswas, Azam, and Lawande [31], where they prove that wave functions belonging to integrable systems can have only one local extremum between two (parallel) nodal lines, thus excluding the possibility of undulations on the surface and hence contour splitting. They argue heuristically that chaotic systems can have surface roughness, a fact strengthened by a careful examination of what the amplitude distribution reveals. The smooth behavior of $P(\psi)$ for a Gaussian amplitude distribution clearly indicates

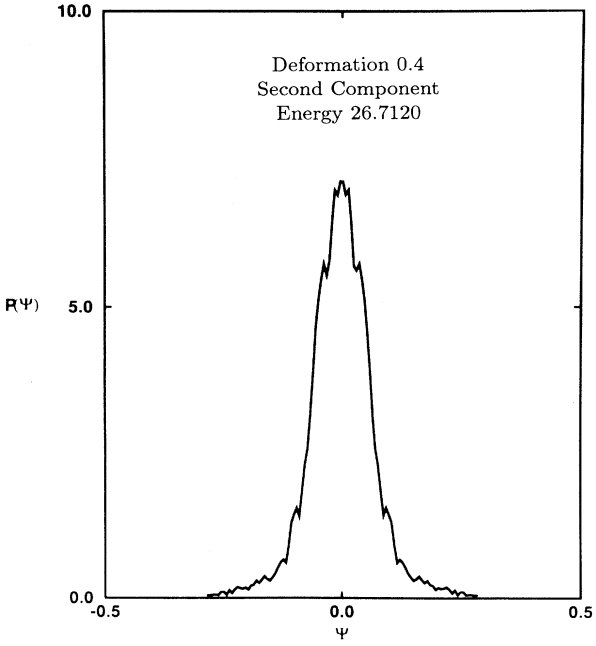

FIG. 16. $P(\psi)$ for the second component of a typical state for $\alpha_2=0.4$.

that there are (nearly) as many points with $\psi=0$ as with ψ equal to a small positive or negative value—a phenomenon that is possible only if the wave function has undulations without crossing zero. Sections of the wave function would then show several contours inside one at a lower "height"—a phenomenon referred to as contour splitting.

In Fig. 15 we first show a plot of amplitude distribution for the first component of the whispering gallery mode in the spherical cavity shown earlier. Since the state is localized, a sharp spike can be seen at zero.

For the 0.4 deformation, however, we present a plot of $P(\psi)$ in Fig. 16 which, though not an ideal Gaussian, exhibits irregularity of the wave functions. We observe, however, that the number of states with an amplitude distribution close to a Gaussian is few since an overwhelming large number of them are scarred. A certain degree of surface roughness can, however, be seen in several cases for the 0.4 deformation case.

V. DISCUSSION

An important aspect of this study has been to understand the nature of the Dirac spectrum. Our results in this direction can be summarized as follows.

(i) Fluctuations in the density of energy eigenstates are due to the same periodic orbits which influence the spectrum for the spinless case.

(ii) The actions S_j associated with the orbits are in general different from the spinless nonrelativistic case and indeed this gives rise to an entirely different spectrum for the Dirac particle.

(iii) Other details such as the dependence of the amplitude of individual oscillations on the repetition number in $d_{\mathrm{fl}}(E)$ seem to be identical to the Schrödinger case.

Not surprisingly, therefore, statistical measures on the spectrum of a spherical cavity belong to the same universality class as a generic spinless nonrelativistic particle having integrable classical dynamics. Further, as is to be expected, these statistical measures approach the results for a spinless nonrelativistic particle having chaotic classical dynamics with increasing deformation of the cavity.

These results naturally give rise to the question of universality in general relativistic systems with spin. Do universality classes exist with respect to the nature of the underlying classical dynamics? Also it is not obvious that the underlying classical dynamics or even the periodic orbits remain unchanged in systems other than cavities or billiards. The work [12] on systems with spin-orbit coupling indicates in that direction. In fact, the equality is a special feature of the cavity potential with hard walls [8]. Particles moving in integrable and nonintegrable potentials need to be considered in future studies.

Our results on wave functions are equally enlightening. Avoided nodal crossings and an increase in irregularity of the curves can be seen with the deformation of the cavity, reminiscent of conventional studies on spinless nonrelativistic systems. Also, the imprint of short periodic orbits on wave functions, a phenomenon referred to as scarring, can be seen in several cases. The orbits involved are identical to those in the spinless case, consistent with our results on the Fourier transform of the spectrum.

Further studies on the wave functions of systems other than cavities are, however, important, since they would indicate any change in the underlying classical dynamics with the introduction of spin.

In conclusion, therefore, our study offers an insight into the nature of the Dirac eigenstates and establishes the influence of periodic orbits in both the quantal energy spectrum and the wave functions.

[1] I. C. Percival, Adv. Chem. Phys. **36**, 1 (1977).
[2] M. C. Gutzwiller, J. Math. Phys. **12**, 343 (1971).
[3] R. Balian and C. Bloch, Ann. Phys. (N.Y.) **69**, 76 (1972); **85**, 514 (1974).
[4] M. V. Berry and M. Tabor, Proc. R. Soc. London Ser. A **349**, 101 (1976).
[5] E. B. Bogomolny, Nonlinearity **5**, 805 (1992); D. Biswas and S. Sinha, Phys. Rev. Lett. **71**, 3790 (1993).
[6] A. O. Barut and N. Zanghi, Phys. Rev. Lett. **52**, 2009 (1984).
[7] A. O. Barut and I. H. Duru, Phys. Rev. Lett. **53**, 2355 (1984).
[8] M. V. Berry and R. J. Mondragon, Proc. R. Soc. London Ser. A **412**, 53 (1987).
[9] Robert G. Littlejohn and William G. Flynn, Phys. Rev. A **44**, 5239 (1991).
[10] Robert G. Littlejohn and William G. Flynn, Phys. Rev. A **45**, 7697 (1992).
[11] Stefan Weigert and Robert G. Littlejohn, Phys. Rev. A **47**, 3506 (1993).
[12] Hans Frisk and Thomas Guhr, Ann. Phys. (N.Y.) **221**, 229 (1993).
[13] A. W. Thomas, in *Advances in Nuclear Physics,* edited by J. W. Negele and E. Vogt (Plenum, New York, 1984), Vol. 13, p. 9.
[14] M. L. Mehta, *Random Matrices* (Academic, New York, 1967).
[15] M. V. Berry and M. Tabor, Proc. R. Soc. London Ser. A **356**, 375 (1977).
[16] O. Bohigas, M. J. Giannoni, and C. Schmit, Phys. Rev. Lett. **52**, 1 (1984).
[17] M. V. Berry, Proc. R. Soc. London Ser. A **400**, 229 (1985).
[18] J. H. Hannay and A. M. Ozorio de Almeida, J. Phys. A **17**, 3429 (1984).
[19] Note that the shapes at some peak positions are exactly out of phase though of the same shape and size. In other words, they would not contribute to the Fourier transform of the combined spectra. Such peaks correspond to half-complete orbits which appear as a consequence of the reflection symmetry of the Hamiltonian. The very first peaks at both the deformations are of this nature and they correspond exactly to half the path lengths of the periodic orbits in the XY plane at $Z=0$ through the origin, which are also the shortest periodic orbits.

[20] D. Biswas, M. Azam, and S. V. Lawande, Phys. Rev. A **44**, 4911 (1991).
[21] S. W. McDonald and A. N. Kaufman, Phys. Rev. A **37**, 3067 (1988).
[22] M. V. Berry, in *Chaotic Behaviour of Deterministic Systems,* edited by G. Iooss, R. G. H. Helleman, and R. Stora (North-Holland, Amsterdam, 1983).
[23] E. J. Heller, Phys. Rev. Lett. **53**, 1515 (1984).
[24] E. B. Bogomolny, Physica D **31**, 169 (1988).
[25] M. V. Berry, Proc. R. Soc. London Ser. A **423**, 219 (1989).
[26] B. Eckhardt, G. Hose, and E. Pollak, Phys. Rev. A **39**, 3776 (1989).
[27] M. Shapiro, D. D. Taylor, and P. Brumer, Chem. Phys. Lett. **106**, 325 (1984).
[28] D. Biswas and S. R. Jain, Phys. Rev. A **42**, 3170 (1990).
[29] M. V. Berry, J. Phys. A **10**, 2083 (1977).
[30] D. Biswas, M. Azam, and S. V. Lawande, Phys. Lett. A **155**, 117 (1991).
[31] D. Biswas, M. Azam, and S. V. Lawande, J. Phys. A **25**, 1735 (1992).